Split-winding type three limb core structured HF transformer for integrating PV and energy storage(ES)

R. Chattopadhyay, G. Gohil and S. Bhattacharya

- ***Published in:*** IEEE Applied Power Electronics Conference and Exposition (APEC), Tampa, FL, 2017
- ***DOI:*** 10.1109/APEC.2017.7931123
- ***Publication date:*** 2017
- ***Citation for published version:*** R. Chattopadhyay, G. Gohil and S. Bhattacharya, "Split-winding type three limb core structured HF transformer for integrating PV and energy storage(ES)," 2017 IEEE Applied Power Electronics Conference and Exposition (APEC), Tampa, FL, 2017, pp. 2997-3004.

Split-Winding Type Three Limb Core Structured HF Transformer for Integrating PV and Energy Storage(ES)

Ritwik Chattopadhyay, Ghanshyamsinh Gohil, Subhashish Bhattacharya
FREEDM Systems Centre, Department of ECE
North Carolina State University
Raleigh, NC, USA
email: rchatto,gvgohil,sbhatta4@ncsu.edu

***Abstract*— The work presented in this paper focuses on the drawbacks of three limb three winding transformer for use in three port dc-dc converter and proposes a split-winding type transformer approach using three limb core for use in three port dc-dc converter. The three limb three winding type transformer has drawback due to limitation of power flow when one port is idle and also has a very limited ZVS operating region for phase shift control. The proposed split-winding type transformer has the equivalent circuit of single core based transformer, has no limitation of power flow when one of the three port is idle and has wide ZVS range. Detailed analysis for idle condition operation, equivalent circuit derivation and ZVS operating range analysis is carried out in this paper.**

Keywords —Split-Winding, Three Limb Three Winding, High Frequency Transformer, Triple Active Bridge, ZVS, SiC Mosfet.

I. INTRODUCTION

Grid integration of Renewable Energy Sources(RES) at medium voltage levels, starting from 4.16kV to 13.8kV, require either a medium voltage inverter with high dc voltage(starting from 6kV and upto 20kV or higher) or the integration could be achieved with the help of a Cascaded H-bridge converter. The use of very high voltage(>10kV) switching devices for two-level, three-level or multi-level converters are essential for withstanding the full dc bus voltage in order to availing a high dc bus voltage(6kV or higher)[1][2]. In a different way, the high dc bus voltage can also be achieved by using several number of series connected low voltage dc buses[3]. Converters with very high voltage SiC devices like 10kV/15kV, have lot of challenges related to high voltages[4] and their reliability have not been proven and are not available for commercial use. The 1200V and 1700V SiC Mosfets, with a maximum safe continuous operating voltage of 1200V-1300V, are used more in number than 10kV/15kV devices and have lesser complexities compared due to much lower voltage of operation. For large scale Photovoltaic(PV) configuration, the use of the series connected multiple dc buses from individual converters, to achieve a high medium voltage dc bus, similar to [3], is more realistic than using a single converter for very high voltage.

For large scale PV installations, integration of Energy Storage(ES) has the potential to play a critical role for smoothening power output. The integration of PV and ES at the dc side, at the modular building block level for large converters, provide the flexibility to control the power output of each individual modular block. For series connected configuration, the output voltage of the modular block can also be controlled along with MPPT. While using only PV(without ES), at modular block level, necessitates extra action to balance the voltage output of each modular block.

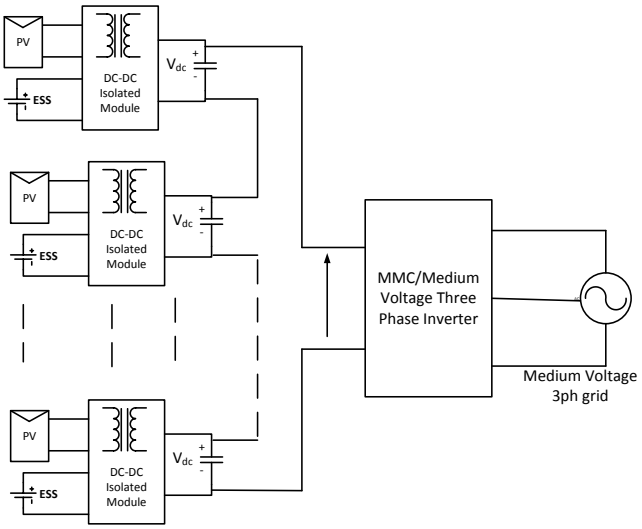

Fig. 1. Large Scale PV Installation Using PV and ES Integrated Blocks

The modular building block dc-dc converter, shown in figure 1, integrating PV and ES for large scale integration, similar to discussed architecture in [3][5], is a crucial part of the architecture. Each dc-dc converter of figure 1 performs the function of power smoothening, power storage and power delivery. One of the important aspect of the modular block dc-dc converter is the high frequency isolation transformer. The power transfer capability, power control, common mode leakage current depend on the high frequency transformer. For all power electronic applications, the common mode leakage current plays a crucial important role in terms of converter performance, EMI etc. The major source of the common mode is the turn-on and turn-off dv/dt of the switching devices[4]. The 1200V and 1700V SiC devices have high dv/dt during switching transitions[6][7]. The galvanic isolation provides high impedance to this leakage current but due to non-idealities in transformer, sufficient inter-winding parasitic capacitance are present due to winding and core geometry, material etc. This capacitance coupled with high dv/dt causes high Cdv/dt common mode leakage current to flow from one port of the transformer to the other port. A method of reducing the inter-winding transformer capacitance is to place the windings on different limbs[8]-[13]. A three limb three winding transformer

prototype(shown in figure 2,5), integrating PV and ES using a Triple Active Bridge Converter, is discussed in [10]-[13]. The three limb three winding transformer has the advantage of very low inter-winding capacitance(around 20-30pF), due to sufficient physical distances between windings, as discussed in [13]. The Triple Active Bridge Converter, using three limb three winding transformer prototype, has few drawbacks in terms of power flow control during idle condition(when one of the port is inactive) and have limited ideal ZVS operating region(ideal ZVS operation neglects the effect of line inductance and device capacitance), as discussed in [10]-[12].

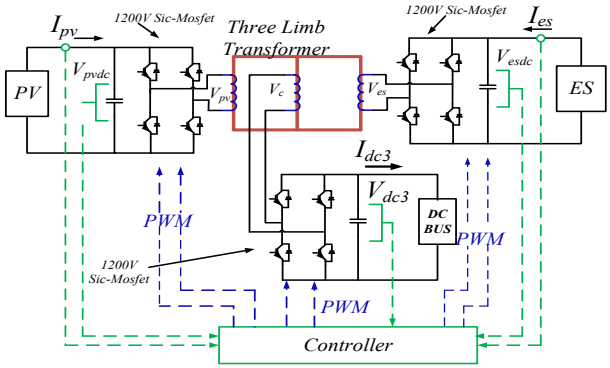

Fig. 2. Three Limb Three Winding Transformer Based Converter

The work presented in this paper, analyzes the drawbacks of using a Triple Active Bridge Converter operation using three limb three winding transformer operation and proposes a suitable transformer prototype while retaining the advantages of low parasitic capacitance of three limb three winding transformer.

II. Drawbacks of Three-Limb Three Winding Transformer Based Triple Active Bridge Converter

A. One Port Idle Operation

One of the most important aspect of operating a three port converter, is its successful operation when 'one port is idle'. For the three limb three winding transformer of figure 2,5, under the scenario of idle condition of one port, the converter attached to the idle port is kept switched off or the winding is kept open, in which case an open circuit voltage develops across the winding. In 'switched off" condition, gate signals for all the controlled semiconductor devices are withdrawn, and the dc source/storage are available but all passive loads are withdrawn from dc buses. During idle condition, as the idle port converter does not provide any excitation to the winding on that core limb, the reluctance offered is very low in that particular limb due to low permeability, and the limb acts very nearly as air core or a short to the flux path. As a consequence, the mmf sources from the other two limbs, see a low reluctance path through the third limb with open winding, and majority of their fluxes flow through the low reluctance path. A very small portion of flux links the two active windings. This phenomenon is shown in figures 3,4. In figure 3, when one side port is open, most of the fluxes from both the windings flow through side limb and a very small mutual flux flows through the middle limb. Similarly, in figure 4, the fluxes from both the limbs flow through middle limb and a very small portion link both the windings.

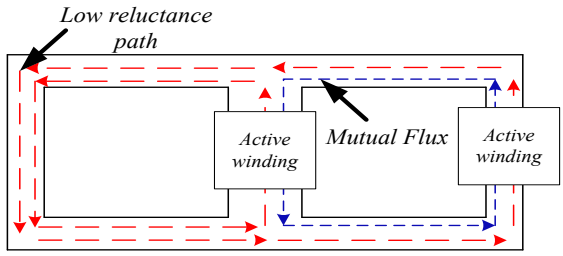

Fig. 3. Flux paths During One Side Port Idle Condition

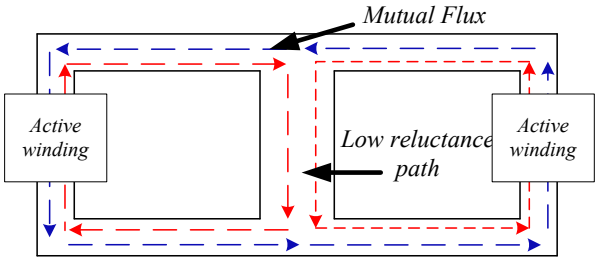

Fig. 4. Flux paths During Middle Port Idle Condition

MATLAB/PLECS simulation of the system shown in figure 2 is carried out to analyze the idle conditions. The transformer details for the three limb transformer of figure 2,5 is given in table 1. A picture of the three limb transformer is shown in figure 5, which is built using 2 stacks of E100/60/28 E cores. The equivalent circuit for MATLAB/PLECS, of three limb three winding transformer is shown in figure 6.

Fig. 5. Three Winding Three Limb Transformer Prototype

TABLE 1

Design Frequency of Operation, B_{max}	50kHz,0.2T
Voltage and no of turns on PV side (V_{pv},N_{pv})	700V, 24
Voltage and no of turns on ES side (V_{es},N_{es})	700V, 24
Voltage and no of turns on Middle port (V_c,N_c)	1200V, 20
Magnetizing inductance from middle port L_m	1.53µH
Leakage Inductance L_{Lpv}, L_{Les}	51.65µH
Leakage inductance L_{Lc}	59µH
Inter-winding capacitance: PV to middle(C_{13})	24pF
Inter-winding capacitance: ES to middle(C_{23})	23pF
Inter-winding capacitance: PV to ES(C_{12})	20pF

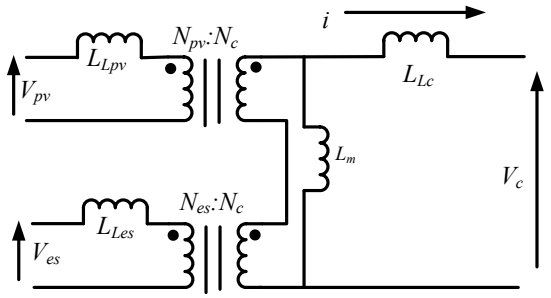

Fig. 6. Electrical Equivalent Circuit for Three Limb Transformer

The one port idle condition simulation is performed by keeping the converter switched off for idle port. Figure 7 shows the winding voltages when one of the side winding in open and the middle port dc bus is connected to a resistive load bank.

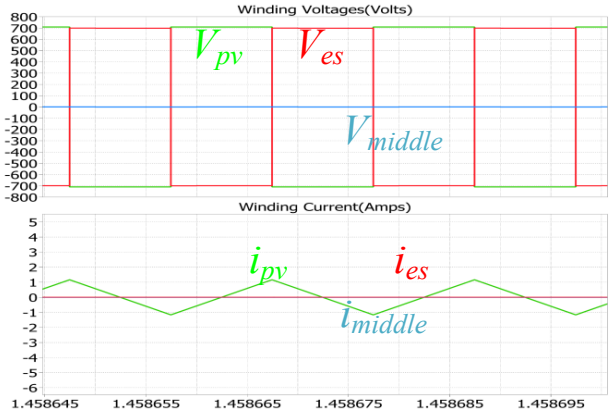

Fig. 7. Winding Voltage and Current when One Side Port is Idle

It can be observed from figure 7, that the voltage developed across middle winding is very low, and only magnetizing current flows through the active port windings. Very low middle winding voltage and high lagging current on side limb winding explains that no active power flows from the active side limb port to the middle limb port. Figure 8 shows the transformer waveforms when the middle port is switched off. An open circuit voltage is developed across middle winding and zero load current flows. The side limb winding currents are purely magnetizing in nature(lag the voltages by 90 degrees) and zero current flows in middle winding, which refers to the fact that very low active power flows from one side limb port to the other. This phenomenon is explained by the low reluctance for the limb with open winding, through which majority of the fluxes flow.

The idle port winding phenomenon is examined by experimental study results, (a)where the PV port is kept idle and the middle port and ES port are active(figure 7), and (b) the middle port is kept idle and PV and ES ports are active(figure 8). In figure 9, the PV port is idle, when very low output power flows from ES port to middle limb port for phase shift of 50 degrees, as the middle port develops very low voltage, similar to that in figure 5. In figure 10, the middle port is kept idle, while PV and ES ports are active, but the windings currents in PV and ES ports are magnetizing in nature and zero current flows through middle winding. Thus very low power flows from PV to ES port despite a phase shift of 30 degree between them. The ringing in winding current is present due to zero resistive load(low damping) in middle port dc bus.

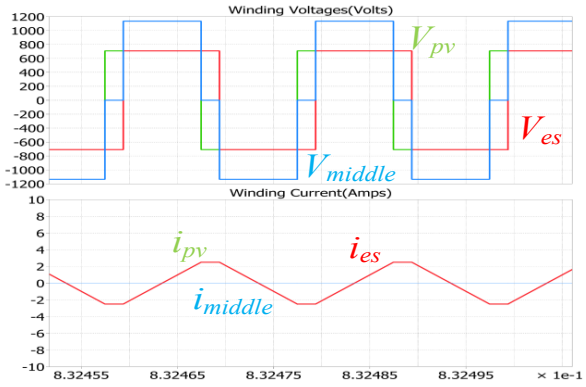

Fig. 8. Winding Voltage and Current when Middle Port is Idle

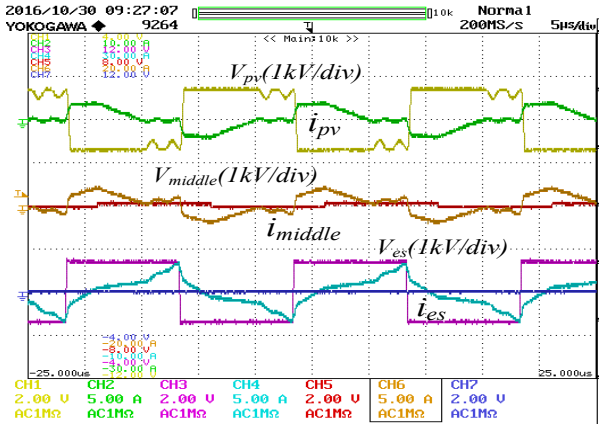

Fig. 9. Winding Voltage and Current when PV Port is Idle

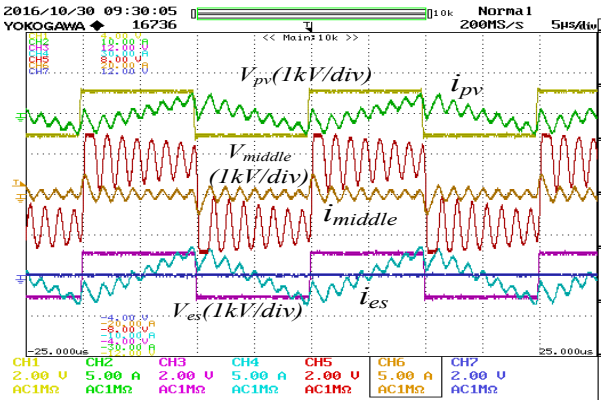

Fig. 10. Winding Voltage and Current when Middle Port is Idle

B. ZVS Operaating Region using Phase Shift Control

One of the most significant characteristics for triple or dual active bridge converters has been the natural ZVS turn-on which offers a significant advantage in converter efficiency at higher frequencies compared to hard-switched converters. The ZVS turn-on is crucial for SiC-Mosfet based converters, as the Mosfet's turn-on losses include both the turn-on and turn-off energy, and the actual Mosfet turn-off loss is quite low. The ZVS operation for any switching leg depend on the direction of

current during switching and the energy stored in inductor and device capacitor. In ideal ZVS turn-on scenarios where the ZVS operation depends only on winding current direction, and it is assumed that the energy stored the inductor is high enough to discharge the device capacitance. Using the ideal condition for ZVS, the operating points are evaluated from the equivalent circuit of figure 6. The full ZVS operating points for converter of figure 2, as a function of phase shift angles ϕ_{pv} and ϕ_{es} of PV and ES port converter, is highlighted in blue color in figure 11, for the operating range of (-π/2 to π/2).

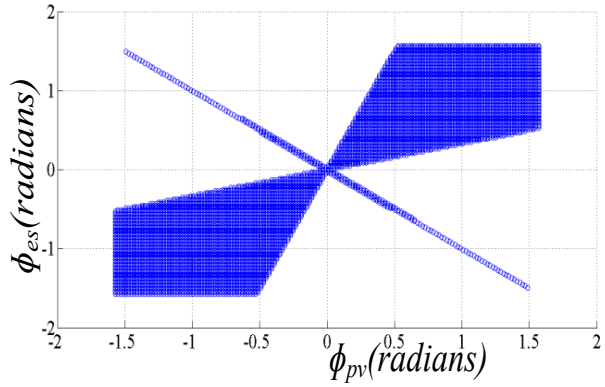

Fig. 11. ZVS Operating Points for Triple Active Bridge Converter Using Three Limb Three Winding Transformer

From figures 11, it can be observed that the ZVS operating points for the triple active bridge converter of figure 2 are limited, and ZVS is achievable when both the phase shift angles are close to each other.

III. Proposed Split-Winding Type Three Port Transformer for Triple Active Bridge Converter

A. Split-Winding Transformer Equivalent Circuit Model

In this section, a split-winding type transformer approach is proposed to eliminate the two major drawbacks of three limb three winding transformer based three port converter. The low reluctance flux path scenario during idle condition and the limitation of ZVS operating points in (-π/2,π/2) region using two phase shift angles ϕ_{pv} and ϕ_{es}, are eliminated using a split-winding approach as shown in figure 12. In split-winding transformer, the PV and ES windings are split up into two and the two sections are placed on the two side limbs. Figure 13 shows the split-winding transformer based dc-dc converter.

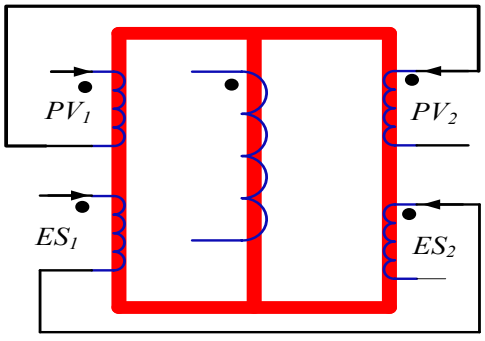

Fig. 12. Split-Winding Transformer Schematic

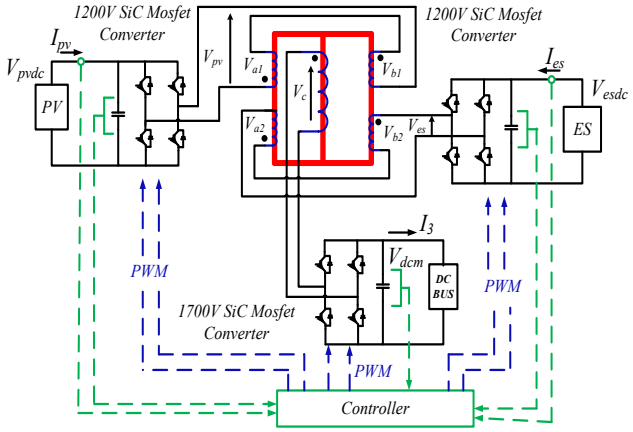

Fig. 13. Split-Winding Transformer enabled TAB Converter

The magnetic equivalent circuit of split-winding transformer is shown in figure 14, from which the flux equation is derived as given in (1).

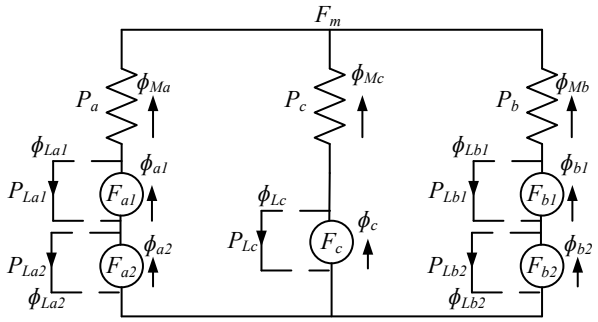

Fig. 14. Magnetic Equivalent Circuit of Split-Winding Transformer

$$\begin{bmatrix}\phi_{a1}\\ \phi_{a2}\\ \phi_{b1}\\ \phi_{b2}\\ \phi_c\end{bmatrix}=\frac{1}{(P_a+P_b+P_c)}\begin{bmatrix}P_a(P_b+P_c) & P_a(P_b+P_c) & -P_aP_b & -P_aP_b & -P_aP_c\\ P_a(P_b+P_c) & P_a(P_b+P_c) & -P_aP_b & -P_aP_b & -P_aP_c\\ -P_aP_b & -P_aP_b & P_b(P_a+P_c) & P_b(P_a+P_c) & -P_bP_c\\ -P_aP_b & -P_aP_b & P_b(P_a+P_c) & P_b(P_a+P_c) & -P_bP_c\\ -P_cP_a & -P_cP_a & -P_cP_b & -P_cP_b & P_c(P_a+P_b)\end{bmatrix}\begin{bmatrix}F_{a1}\\ F_{a2}\\ F_{b1}\\ F_{b2}\\ F_c\end{bmatrix}$$
$$+\begin{bmatrix}P_{La1} & & & & \\ & P_{La2} & & & \\ & & P_{Lb1} & & \\ & & & P_{Lb2} & \\ & & & & P_{Lc}\end{bmatrix}\begin{bmatrix}F_{a1}\\ F_{a2}\\ F_{b1}\\ F_{b2}\\ F_c\end{bmatrix} \quad (1)$$

Equation (1) can be modified to represent the electrical equivalent form as given in (2), where the inductances are actually functions of the permeances from (1). The electrical equivalent circuit as derived from (2), is shown in figure 15. Since the split portions are connected in series as shown in figures 12-13, the reduced order electrical equivalent circuit is shown in figure 16 and the reduced matrix is given in (3).

$$\begin{bmatrix}V_{a1}\\ V_{a2}\\ V_{b1}\\ V_{b2}\\ V_c\end{bmatrix}=\begin{bmatrix}L_{a1a1} & L_{a1a2} & -L_{a1b1} & -L_{a1b2} & -L_{a1c}\\ L_{a2a1} & L_{a2a2} & -L_{a2b1} & -L_{a2b2} & -L_{a2c}\\ -L_{b1a1} & -L_{b1a2} & L_{b1b1} & L_{b1b2} & -L_{a1c}\\ -L_{b2a1} & -L_{b2a2} & L_{b2b1} & L_{b2b2} & -L_{b2c}\\ -L_{ca1} & -L_{ca2} & -L_{cb1} & -L_{cb2} & L_{cc}\end{bmatrix}\frac{d}{dt}\begin{bmatrix}i_{a1}(t)\\ i_{a2}(t)\\ i_{b1}(t)\\ i_{b2}(t)\\ i_c(t)\end{bmatrix} \quad (2)$$

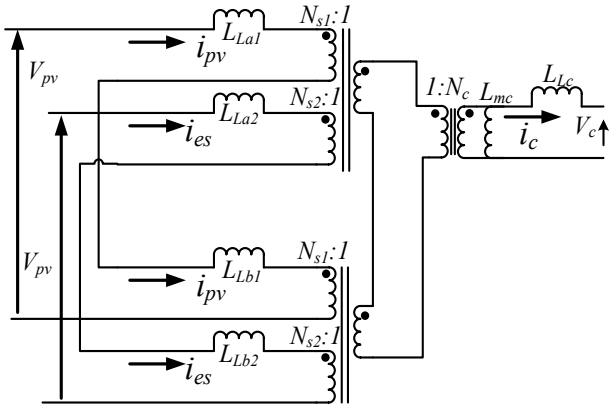

Fig. 15. Electrical Equivalent Circuit of Split-Winding Transformer

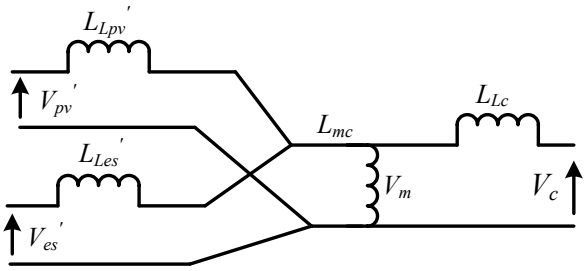

Fig. 16. Reduced Order Electrical Equivalent Circuit

$$\begin{bmatrix} V_{pv} \\ V_{es} \\ V_c \end{bmatrix} = \begin{bmatrix} L_{pvpv} & L_{pves} & -L_{cpv} \\ L_{pves} & L_{eses} & -L_{ces} \\ -L_{cpv} & -L_{ces} & L_{cc} \end{bmatrix} \frac{d}{dt} \begin{bmatrix} i_{pv}(t) \\ i_{es}(t) \\ i_c(t) \end{bmatrix} \quad (3)$$

$$L_{Lpv}' = \left(\frac{N_c}{N_{s1}}\right)^2 (L_{La1} + L_{Lb1}) \quad (4), \quad L_{Les}' = \left(\frac{N_c}{N_{s2}}\right)^2 (L_{La2} + L_{Lb2}) \quad (5)$$

$$V_{pv}' = \left(\frac{N_c}{N_{s1}}\right) V_{pv} \quad (6), \qquad V_{es}' = \left(\frac{N_c}{N_{s2}}\right) V_{es} \quad (7)$$

From the reduced order equivalent circuit model, it can be inferred that the model is similar to single core based three winding transformer, as discussed in [14]. The power flow control for the split-winding transformer is similar to that discussed in [14].

B. Split-Winding Transformer Parameters

A split-winding transformer is designed with same core, same size and same design parameters(such as flux density, operating freuqency) as used for three limb transformer in section 2 by joining two E-100/60/28 cores stacked together, as shown in figure 17. The number of turns for the split sections are half of the total number of turns for three limb transformer of figure 5. The transformer parameter details are given in table 2. Figure 18 gives the capacitive model for the split-winding transformer. From table 2, it can be observed that the inter-winding parasitic capacitances are close to that of three limb three winding transformer, thus retaining the advantage of low inter-winding parasitic capacitances for split-winding approach.

Fig. 17. Split-Winding Transformer Prototype

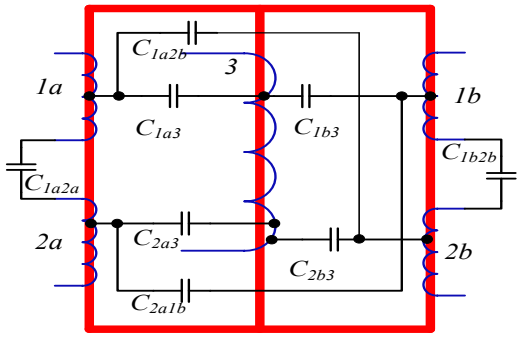

Fig. 18. Split-Winding Transformer Capacitance Network

TABLE 2	
Design Frequency of Operation, B_{max}	50kHz,0.2T
Voltage and no of turns on split sections of PV port *(V_{pv},N_{s1})*	700V, 12
Voltage and no of turns on split sections of ES port *(V_{es},N_{s2})*	700V, 12
Voltage and no of turns on Middle port *(V_c,N_c)*	1200V, 20
Magnetizing inductance from middle port L_m	1.15mH
Leakage Inductance for PV: L_{Lpv}=(L_{La1}+L_{Lb1})	33µH
Leakage Inductance for ES: L_{Lpv}=(L_{La2}+L_{Lb2})	37µH
Leakage Inductance for Middle : L_{Lc}	88 µH
Inter-winding capacitance : $C_{1a\text{-}3}$, $C_{2a\text{-}3}$	17pF,18pF
Inter-winding capacitance : $C_{1b\text{-}3}$, $C_{2b\text{-}3}$	14pF,16pF
Inter-winding capacitance : $C_{1a\text{-}2a}$, $C_{1b\text{-}2b}$	5pF,7pF
Inter-winding capacitance : $C_{1a\text{-}2b}$, $C_{1b\text{-}2a}$	3pF, 4pF

C. One Port Idle Condition Operation

The one port idle condition scenarios are analyzed in a similar way here for split-winding transformer based triple active bridge converter, similar as in previous section. The flux paths for the split-winding transformer are shown for three cases as in figure 19-21.

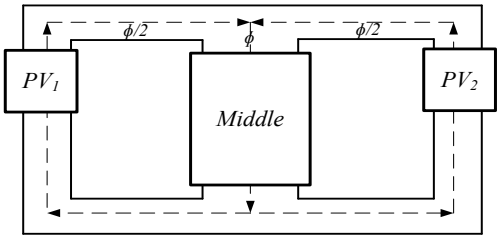

Fig. 19. Flux Flow Path when ES Port is Idle or Open

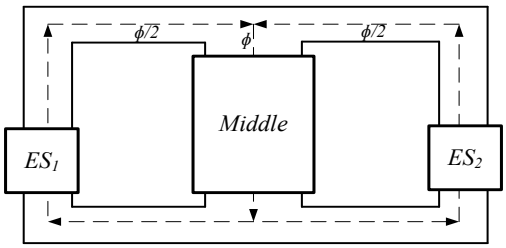

Fig. 20. Flux Flow Path when PV Port is Idle or Open

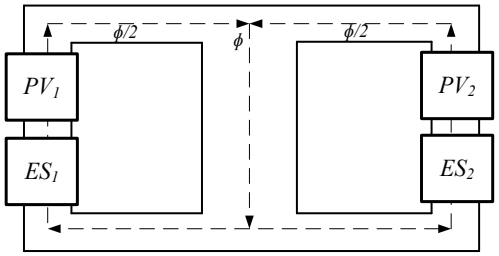

Fig. 21. Flux Flow Path when Middle Port is Idle or Open

For the three cases shown in figures 19-21, during one port idle scenario, the flux induced by one active winding completely links or cuts across the other active winding, and all the limbs are equally excited as middle limb has generally a cross-section area double than that of side limb area. MATLAB/PLECS simulation has been carried out using PLECS magnetic circuit model to observe the one port idle scenarios. In idle mode, the converter is kept switched off and for middle port the dc load is removed from the idle port dc bus. Figures 22-24 show the three different cases for one port idle scenario. It can be observed that an open circuit voltage develops across the idle winding while the current in the idle winding is zero. Also, during this scenario, it can be observed that the active ports have winding current which are in phase or out of phase, indicating successful power flow between active ports. The same scenarios have been examined with experimental study as shown in figures 25-27. In experimental waveforms as well, the idle port winding develops a voltage across it and carries zero current while the active ports take part is successful power flow between them. In experimental study for ES and PV ports, the dc sources are kept attached to the dc bus during idle condition, and no ringing develops on PV and ES winding voltages(figures 25-26). Whereas for middle port idle condition, the dc loads are removed, thus very low damping is present in middle port, causing high ringing in winding voltage(figure 27). The successful operation of active ports during one port idle scenario can be confirmed from the simulation and experimental results.

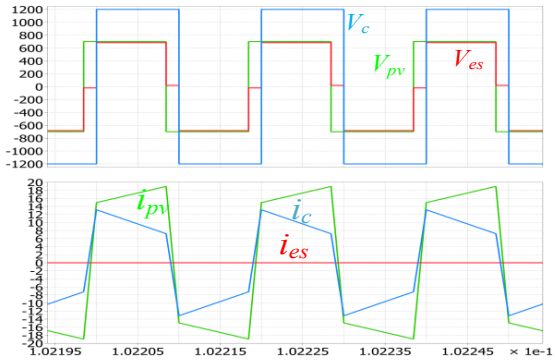

Fig. 22. Transformer Winding Waveforms when ES Port is Idle

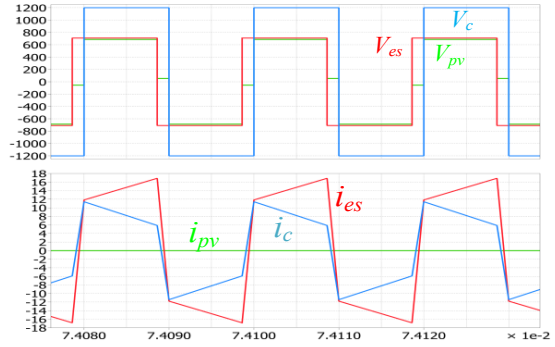

Fig. 23. Transformer Winding Waveforms when PV Port is Idle

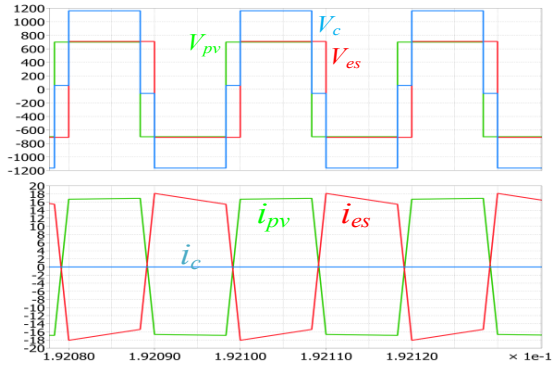

Fig. 24. Transformer Waveforms when Middle Port is Idle

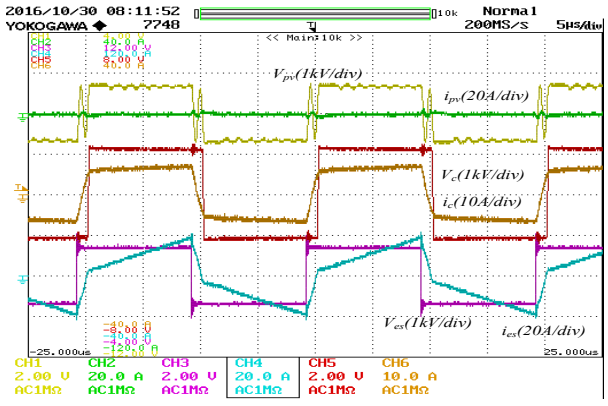

Fig. 25. Transformer Winding Waveforms when PV Port is Idle.

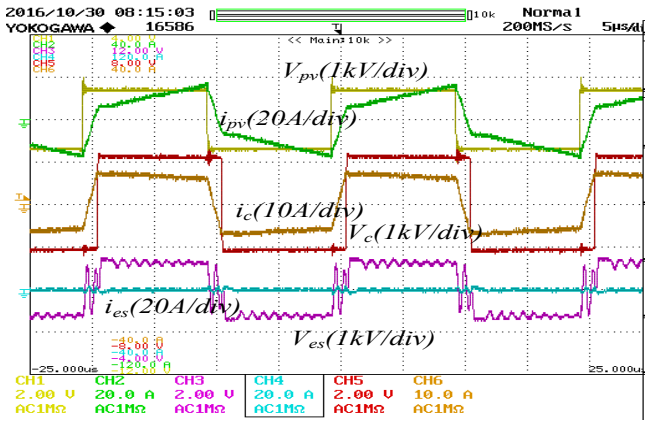

Fig. 26. Transformer Winding Waveforms when ES Port is Idle.

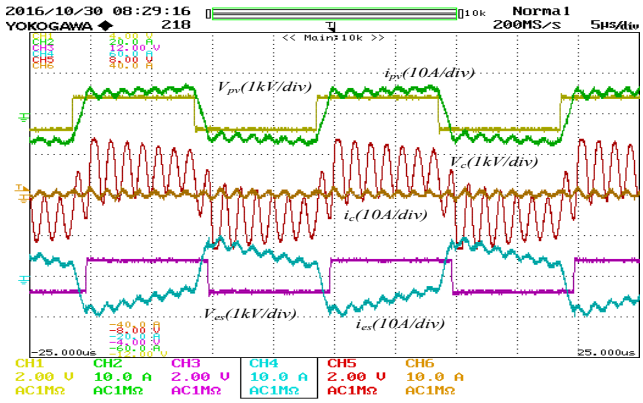

Fig. 27. Transformer Waveforms when Middle Port is Idle

D. ZVS Operating Range Using Split-Winding Transformer

The full ZVS operation range for ideal ZVS turn-on case, the three port triple active bridge converter is shown in figure 28 for both PV converter and ES converter phase shift angles ϕ_{pv} and ϕ_{es} in the operating range of (-π/2, +π/2). It can be observed that the split-winding transformer provides a much larger ZVS operating range for the triple active bridge converter. The ZVS ranges are evaluated by solving current expression in terms of phase shift angles from equivalent circuit of figure 16.

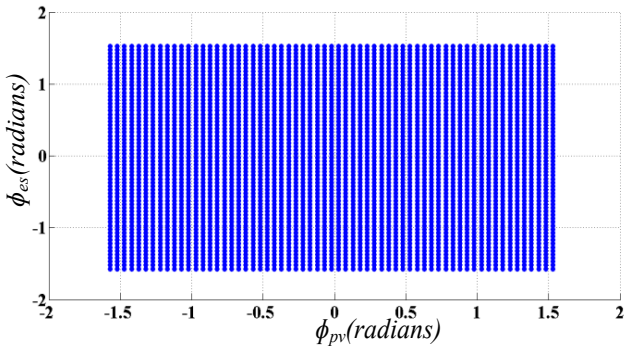

Fig. 28. ZVS Operating Points for Triple Active Bridge Converter Using Split-Winding Type Three Winding Transformer

Figures 29-32 show experimental waveforms for transformer winding voltages and currents for different ZVS turn-on cases during low and high power outputs. The ZVS turn-on scenarios are identified with negative outgoing currents during $-V_{dc}$ to $+V_{dc}$ transition in winding voltages for PV and ES ports, and with positive incoming current for middle port during $-V_{dc}$ to $+V_{dc}$ voltage transition.

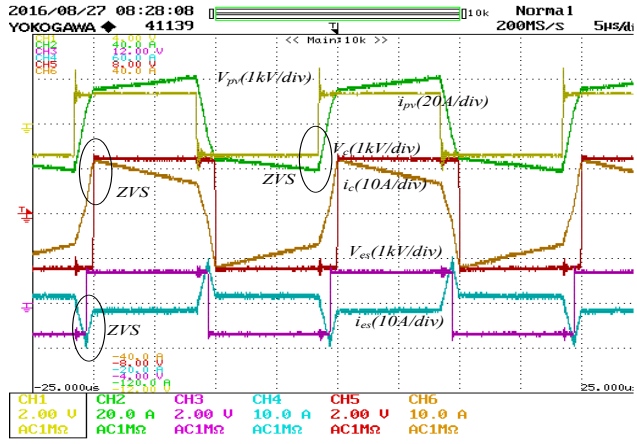

Fig. 29. PV delivers 12kW, ES charges with 2.4kW

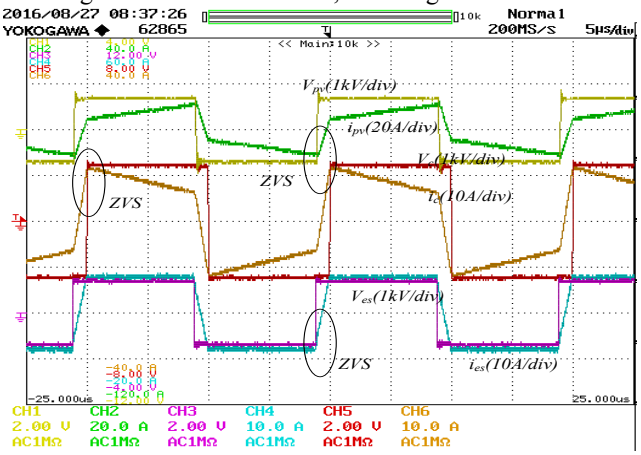

Fig. 30. PV delivers 4.5kW, ES delivers 5kW

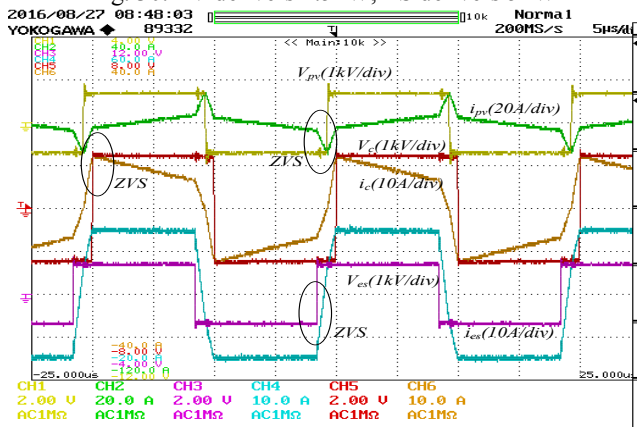

Fig. 31. PV delivers 1.2kW, ES delivers 8.3kW

Figures 29-30 show the ZVS turn-on cases when PV delivers and ES charges or discharges. Figures 31 show the case when PV delivers very low power but still having ZVS and figure 32 show the case when ES delivers low power while still having ZVS turns-on.

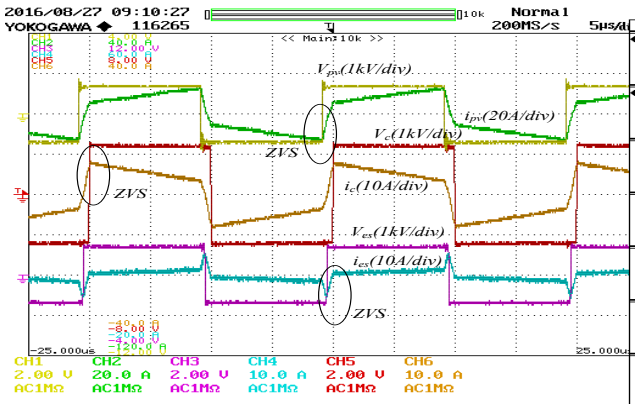

Fig. 32. PV delivers 5.2kW, ES delivers 1.2kW

The system efficiencies are compared for the two transformer prototypes using the same converter setup using SiC Mosfets of 1200V and 1700V. When ES is delivering power, then $P_{in} = P_{pv} + |P_{es}|$, $P_{out} = P_c$ and while ES is charging, $P_{in} = P_{pv}$, $P_{out} = P_c + |P_{es}|$. The efficiency of the converter is defined as $\eta = P_{out}/P_{in}$. Figures 33 and 34 show efficiency curve for the two transformer prototype based converter at 50lHz switching frequency. All the measured data are taken from 5 minutes continuous run of the converter.

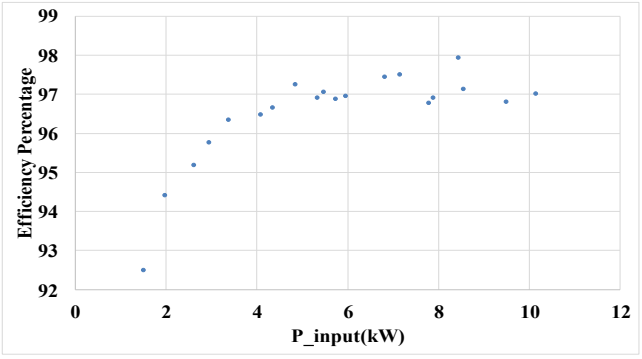

Fig. 33. System Efficiency Plot for Three Limb Three Winding

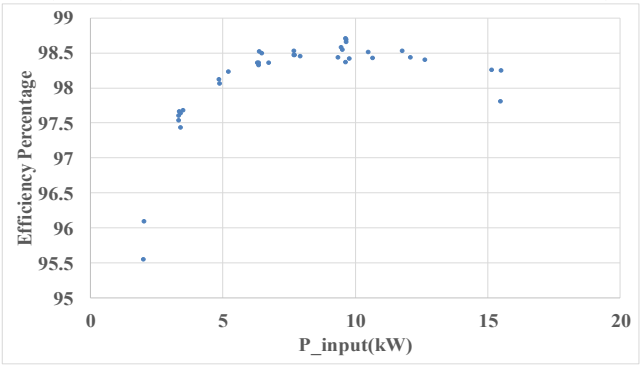

Fig. 34. System Efficiency Plot for Three Limb Split-Winding

CONCLUSIONS

From the above results, it can be observed that the split-winding transformer based three port converter is able to overcome the drawbacks of three limb three winding transformer based converter, mainly the operation during one port idle condition and loss of ZVS operating points, while the inter-winding parasitic capacitances are still kept at significantly lower values(around 10-20pF). The split-winding transformer approach provides higher efficiency(by 0.5-1%) than three limb three winding approach due to larger ZVS ranges for same transformer size, design parameters and same test setup.

REFERENCES

[1] Q. Zhu, Li Wang, L. Zhang, W. Yu, A. Q. Huang, "Improved medium voltage AC-DC rectifier based on 10kV SiC MOSFET for Solid State Transformer (SST) application," *IEEE Applied Power Electronics Conference and Exposition (APEC), 2016*, pp. 2365 – 2369.

[2] D. Rothmund, G. Ortiz, Th. Guillod, J. W. Kolar, "10kV SiC-based isolated DC-DC converter for medium voltage-connected Solid-State Transformers," *IEEE Applied Power Electronics Conference and Exposition (APEC), 2015*, pp. 1096 – 1103.

[3] Azidehak, R. Chattopadhyay, S. Acharya, A.K. Tripathi, M.G. Kashani, G. Chavan, S. Bhattacharya, "Control of modular dual active bridge DC/DC converter for photovoltaic integration," *IEEE Energy Conversion Congress and Exposition (ECCE), 2015,* pp. 3400 - 3406.

[4] A. Tripathi, S. Madhusoodhanan, K. Mainali, A. Kadavelugu, D. Patel, S. Bhattacharya, K. Hatua, "Grid connected CM noise considerations of a three-phase multi-stage SST," *9th International Conference on Power Electronics and ECCE Asia (ICPE-ECCE Asia), 2015,* pp. 793 - 800.

[5] A. Azidehak, N. Yousefpoor, S. Bhattacharya, "Control and synchronization of distributed controllers in modular converters," *IECON 2014 - 40th Annual Conference of the IEEE Industrial Electronics Society(2014),* pp. 3644-3650.

[6] S. Hazra, A. De, L. Cheng, J. Palmour, M. Schupbach, B. Hull, S. Allen, S. Bhattacharya, "High Switching Performance of 1700V, 50A SiC Power MOSFET over Si IGBT/BiMOSFET for Advanced Power Conversion Applications," *IEEE Trans. Power Elec.,* vol. 31, Issue. 16, pp. 4742-4754, Year. 2016.

[7] D. Aggeler, J. Biela, J.W. Kolar, "Controllable dυ/dt behaviour of the SiC MOSFET/JFET cascode an alternative hard commutated switch for telecom applications," *Twenty-Fifth Annual IEEE Applied Power Electronics Conference and Exposition (APEC), 2010*, pp. 1584 – 1590.

[8] S. Dutta, S. Roy, S. Bhattacharya, "A mode switching, multiterminal converter topology with integrated fluctuating renewable energy source without energy storage," in *IEEE Twenty-Ninth Annual Applied Power Electronics Conference and Exposition(APEC)*, 2014, pp. 419-426.

[9] R. Chattopadhyay, S. Bhattacharya, "Modular Isolated DC-DC Converter with Multi-Limb Transformer for Interfacing of Renewable Energy Sources", *in IEEE Applied Power Electronics Conference and Exposition(APEC),* 2015, pp. 3039- 3046.

[10] R. Chattopadhyay, S. Bhattacharya, "Power Flow Control and ZVS Analysis of Three Limb High Frequency Transformer Based Three-Port DAB", *IEEE 2016 Applied Power Electronics Conference and Exposition(APEC), 2016,* pp. 778-785.

[11] R. Chattopadhyay, S. Bhattacharya, "ZVS Analysis and Power Flow Control for Three Limb Transformer Enabled SiC Mosfet Based Three Port DAB Integrating PV and Energy Storage(ES)," *presented at IEEE Energy Conversion Congress and Exposition(ECCE), 2016.*

[12] R. Chattopadhyay, S. Bhattacharya, "Decoupled power flow using phase shift control and ZVS cases for a three limb high frequency transformer based three-port DAB integrating PV and energy storage," *IEEE Industry Applications Society Annual Meeting(IAS), 2016*, pp. 1-8.

[13] R. Chattopadhyay, M.A. Juds, P.R. Ohodnicki, S. Bhattacharya, "Modelling, Design and Analysis of Three Limb High Frequency Transformer Including Transformer Parasitics, for SiC Mosfet Based Three Port DAB," *presented at 42nd Annual IEEE Industrial Electronics Conference (IECON), 2016.*

[14] Z. Chuanhong, J.W. Kolar, "A novel three-phase three-port UPS employing a single high-frequency isolation transformer," *IEEE 35th Annual Power Electronics Specialists Conference(PESC), 2004,* pp. 4135 - 4141.